The Lyot Project: Status and Deployment Plans

Ben R. Oppenheimer, Andrew P. Digby, Laura Newburgh, Douglas Brenner, Michael Shara
Department of Astrophyics
American Museum of Natural History
79th Street at Central Park West
New York, NY 10024
bro@amnh.org
Russell B. Makidon, Anand Sivaramakrishnan, Remi Soummer
Space Telescope Science Institute
3700 San Martin Blvd.
Baltimore, MD 21218
James R. Graham, Paul Kalas, Marshall Perrin
Department of Astronomy
University of California-Berkeley
Berkeley, CA 94720-3411
Lewis C. Roberts, Jr.
AMOS - The Boeing Company
535 Lipoa Pkwy Suite 200
Kihei, HI 96753
Jeffrey Kuhn, Kathryn Whitman
Institute for Astronomy
University of Hawaii
2680 Woodlawn Dr.
Honolulu, HI 96822
James P. Lloyd
Department of Astronomy
California Institute of Technology
105-24, Pasadena, CA 90025

ABSTRACT

For the first time in history, astronomers can image the environments of nearby stars on scales approaching that of our solar system. New classes of astrophysical objects have been discovered including circumstellar debris disks, brown dwarfs, and super-Jupiter mass planets. These discoveries have galvanized intense public interest and have led to profound new insights into the formation and evolution of planetary systems such as our own. Among the key enabling technologies are adaptive optics (AO) and coronagraphy, which deliver the high contrast necessary for the discovery and characterization of faint stellar companions and circumstellar disks in the solar neighborhood. Among the AO systems available to astronomers, AEOS is unique because it delivers very high order wave front correction. The Lyot Project includes the construction and installation of an AEOS-optimized coronagraph that exploits the full astronomical potential of AEOS and represents a critical step toward the long-term goal of directly imaging and studying extrasolar planets (a.k.a. ``exoplanets''). We provide an update on the Project, whose coronagraph will be installed at AEOS in October 2003, and whose infrared camera saw first light in April 2003.

1. INTRODUCTION

For the first time in history, astronomers can image the environments of nearby stars on scales approaching that of our solar system. New classes of astrophysical objects have been discovered including circumstellar debris disks, brown dwarfs, and super-Jupiter mass planets. These discoveries have galvanized intense public interest in science and technology and have led to profound new insights into the formation and evolution of planetary systems such as our own.

Among the key enabling technologies are adaptive optics (AO) and coronagraphy, which deliver the high contrast necessary for the discovery and characterization of faint stellar companions and circumstellar disks in the solar

neighborhood. Among the AO systems available to astronomers, AEOS is unique because it delivers very high order wavefront correction; our program, to build and deploy an AO optimized coronagraph, exploits the full astronomical potential of AEOS and represents a critical step toward the long-term goal of directly imaging and studying extrasolar planets (a.k.a. ``exoplanets").

2. AO CORONAGRAPHY

AO increases angular resolution and more importantly contrast, so that a faint object can be detected close to a bright source that would otherwise overwhelm it. Coronagraphy artificially suppresses the light of a bright star. To quantify the astronomical utility of the proposed coronagraph we consider two factors: 1) the degree of contrast enhancement; 2) the radii at which enhanced contrast is achieved.

1. Consider the contrast improvement when an AO system is used to observe two stars separated by an angle smaller than the seeing disk but larger than the Airy disk. Suppose S_{AO} and S_{see} are the Strehl ratios in corrected and uncorrected images. A useful measure of the contrast improvement, η, is the product of two factors: the ratio S_{AO}/S_{see}, due to sharper images, and the factor, $1/(1- S_{AO})$, due to the amount of light removed by AO from the seeing disk. Hence,

$$\eta = \frac{S_{AO}}{S_{see}} \frac{1}{(1-S_{AO})}$$

For low-order systems (e.g., Palomar or Lick), $S_{AO} \sim 0.5$ and $S_{see} \sim 0.03$, and $\eta \sim 30$. For low Strehls image sharpness is the dominant factor. But as $S_{AO} \rightarrow 1$ large improvements accrue as progressively more light is removed from the seeing disk. The AEOS system has enormous astronomical potential because we predict that it will deliver $S_{AO} \approx 0.89$ in the near-IR at 1.6 μm and give $\eta \geq 300$. This advantage diminishes at shorter wavelengths. For example, at *I*-band (0.9 μm) the Strehl ratio drops to 0.25 and the corresponding contrast enhancement is a factor of thirty less. This steep wavelength dependence, together with our desire to find cool (effective temperature, $T \leq 1000$ K) companions drives the requirement to operate the coronagraph in the near IR. Our prediction is fully supported by actual visible images taken with AEOS.

2. The full improvement in contrast exists only within a radial distance from the star, θ_{AO}, which is determined by the design of the AO system [1]. AO correction can be thought of as a high-pass filter acting on spatial phase variations of incoming wavefronts. The AO system's spatial frequency cutoff is $k_{AO} = N_{act} / 2D$, where N_{act} is the linear number of deformable mirror actuators projected across the primary of diameter D. The electric field at the image and pupil planes are a Fourier pair, so k_{AO} corresponds to an angle $\theta_{AO} = N_{act} \lambda /2D$ on the sky at wavelength λ. Thus AO only improves the point spread function (PSF) within a radius θ_{AO} (within the dotted circle in Fig. 1(b)). The Lick 3-m, Palomar 5-m, and AEOS 3.63-m systems have 8, 16 and 34 actuators projected across their entrance pupil diameters. Thus, on these systems, AO improves a stellar image to distances of 4 (0.4 arcsec), 8 (0.5 arcsec) and 17 (1.5 arcsec) diffraction widths respectively at 1.6 μm (Fig. 1).

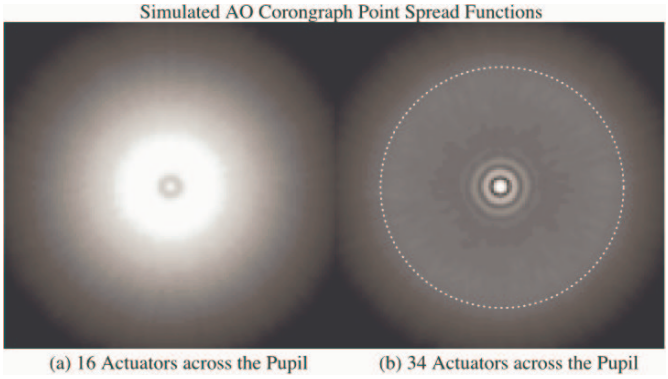

Fig. 1 Comparison of low and high order AO PSFs at 1.6 μm

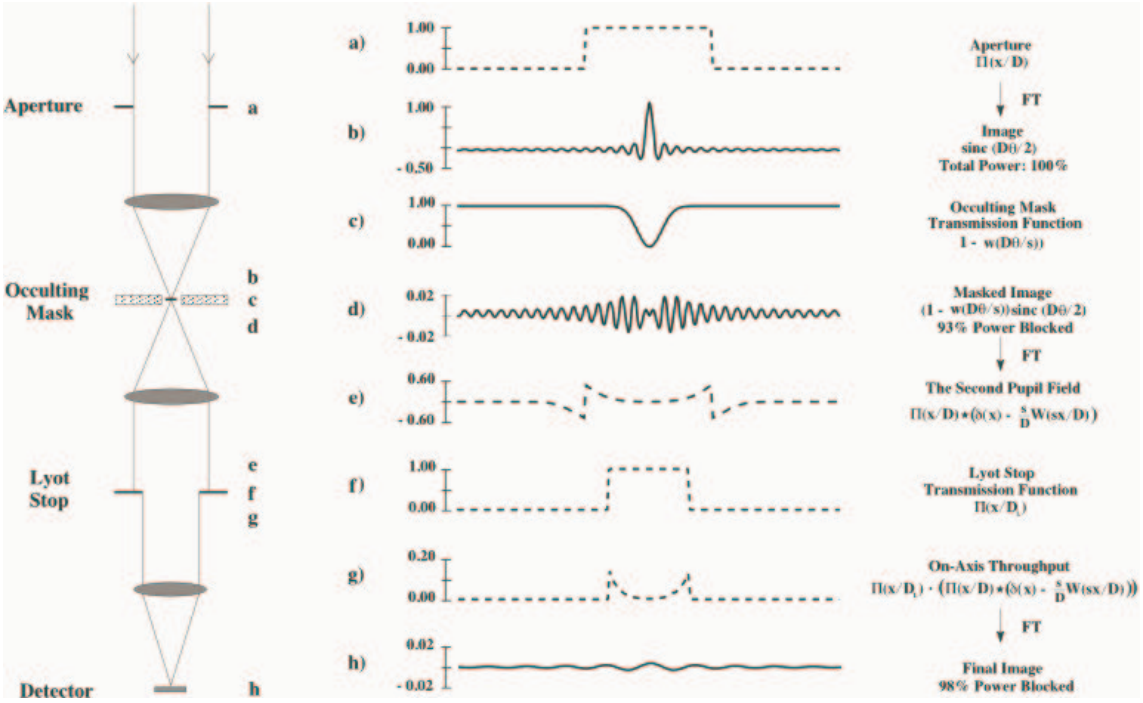

Fig. 2 Principles of coronagraphy. Panels (a)-(h) show the one-dimensional E-fields for an on-axis star and the transmission functions of the optical components. Comparison of the E-fields in image planes (b and d) before and after the focal plane mask (c) show the effects of the occulting disk. The diffraction pattern of the occulted star in the pupil plane (e) is masked by the Lyot stop (f) producing the spatially filtered E-field (g) of the final image (h).

Our science demands high contrast on angular scales corresponding to solar system dimensions (10-30~AU) for nearby stars (10-30 pc) or within the seeing disk at radii of about 1 arcsec. *AO alone cannot achieve the very high dynamic range necessary to find faint companions and circumstellar disks.* This requires a coronagraph. A coronagraph [2], consists of two stops placed in the reimaged focal and pupil planes (Fig. 2) respectively. The focal plane stop (Fig. 2) is an opaque disk, optimally 3 to 9 times the size of the core of the stellar image. This mask blocks most of the on-axis starlight. The effect of this mask on (b) is shown in (d). After the occulting mask, the pupil is reimaged (e), where the remaining starlight is distributed as the Fourier transform of (d). This light is associated with the Airy rings of the image in a periodic spatial distribution; its periodicity is of the order of the telescope's angular resolution (λ/D). Thus, this energy appears predominantly in an annulus at the edges of the pupil (e). The undersized Lyot stop (f) removes this light at the expense of some reduction of the telescope collecting area. In essence, the Lyot stop is a spatial filter that removes the high spatial frequency components of the electric field. The central obscuration scatters light into a similar bright ring around the inner edge of the pupil. The Lyot stop must mask this too, so that a small secondary (such as that on AEOS) is a great advantage. On AEOS an optimized coronagraph lets up to 34% more light through than a similar system on a typical telescope with a secondary diameter a third of that of the primary. The net result is that an on-axis source behind the aperture mask is suppressed by several orders of magnitude relative to an off-axis target.

In an optimized coronagraph the occulting spot must span at least four diffraction widths in diameter. This results in little gain from using a coronagraph with AO systems where $N_{act} < 8$, since the occulting spot occludes most of the improved image area: At Palomar, with a $5\lambda/D$ (0.34 arcsec at 1.6 μm) radius spot, an improved image annulus only $3\lambda/D$ wide (0.20 arcsec) surrounds the spot. For AEOS the image is corrected out to 1.5 arcsec (at 1.6 μm). Thus the light from the central star is suppressed from the edge of the stop at 0.2 to 1.5 arcsec where AO stops improving the image. The consequence is that an order of magnitude more stars can be searched on solar-system scales for companions and disks.

These arguments strongly suggest the tremendous technical potential of a coronagraph designed to exploit AEOS's unique capabilities. We can extend the arguments further to show that large gains in scientific results will follow.

3. WHAT THE AEOS CORONAGRAPH WILL ACHIEVE

To show that an AEOS coronagraph provides a unique and dramatic improvement over existing facilities, and opens an entirely new parameter space in the direct detection of faint companions of nearby stars, we have simulated the performance of the AEOS adaptive optics system with a coronagraph. These simulations include detailed descriptions of atmospherically disturbed wavefronts, the telescope optics (including microroughness and scattered light effects, but neglecting spiders), a Shack-Hartmann wavefront sensor, a square geometry deformable mirror, including the 5 actuators which are inactive in the AEOS beam, the precise sizing and shape of the coronagraph's focal and pupil plane masks, and finally detector characteristics, including read-noise, sky background and quantum efficiency [1].

Clearly we are attempting to simulate a fairly complicated system, with almost 20 optical surfaces. Thus it is critical to establish how meaningful these simulations are. We have compared them with actual, non-coronagraphic, AEOS *I*-band images. (No coronagraphic or IR images exist from this telescope yet.) In this test case, we run the simulations in the *I*-band without the coronagraph. Our simulations reproduce the AEOS PSF shape with a precision of better than 5% out to 3.5 arcsec separation from the stellar locus. Thus, we have accurately included the effects of dust and microroughness on the AEOS optics as well as *all* effects that are important for the science discussed here. The halo-clearing effect of the large number of actuators (cf. Fig. 1) is the most critical element of the PSF that we seek to exploit. This effect is two orders of magnitude larger than the differences between our simulations and actual AEOS data.

Further testing involved additional simulations attempting to show what the Palomar 5-m AO system can achieve. In this case, the real system does have an IR coronagraph whose sensitivity has been evaluated [2, 3]. The simulations of the Palomar AO system and coronagraph match the observations to within 6% at all separations from the primary star.

From the simulations of the AEOS coronagraph, we can determine the 5-σ detection limits for faint point sources injected artificially into the AEOS PSF (Fig. 1(b)). The detection limits are completely determined by the residual light of the star (including speckle noise and photon-shot noise) and are expressed here in terms of dynamic range, the ratio of the flux of the faint companion to that of the bright, occulted primary star. Fig. 3 shows the dynamic range as a function of angular separation from the primary star for an image of 1000 s exposure with the new instrument. The meaning of dynamic range here is such that in 1000 s we can detect a point source up to 14.2 mag. (4.8×10^5) fainter than the primary star within 1.5 arcsec. AEOS will be more sensitive than the existing Palomar AO coronagraph by more than two magnitudes at 0.6 arcsec. Fig. 3 also shows the same curve for a theoretical lower-order AO coronagraph on a similar 3.63-m telescope. Beyond 1.5, AEOS and the lower-order systems are roughly matched in sensitivity. The AEOS sensitivity will also be about 7 mag. better than the Hubble Space Telescope's WFPC2 survey for faint companions of nearby stars [4].

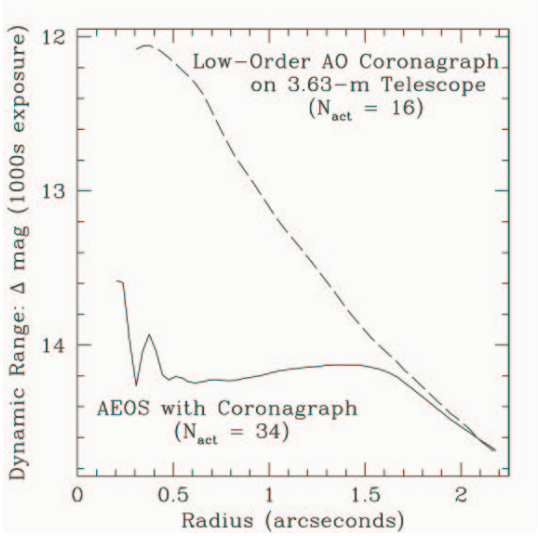

Fig. 3 Dynamic range for a 1000 s exposure with the AEOS coronagraph

4. OPTOMECHANICAL DESIGN

The coronagraph, currently under construction in New York at the American Museum of Natural History, is scheduled to ship to Maui in the Fall of 2003, where it will be used in AEOS's Experiment Room 6. The coronagraph feeds an f/71 beam to the IR science camera, currently under construction in Hawaii by PB, JK and DP.

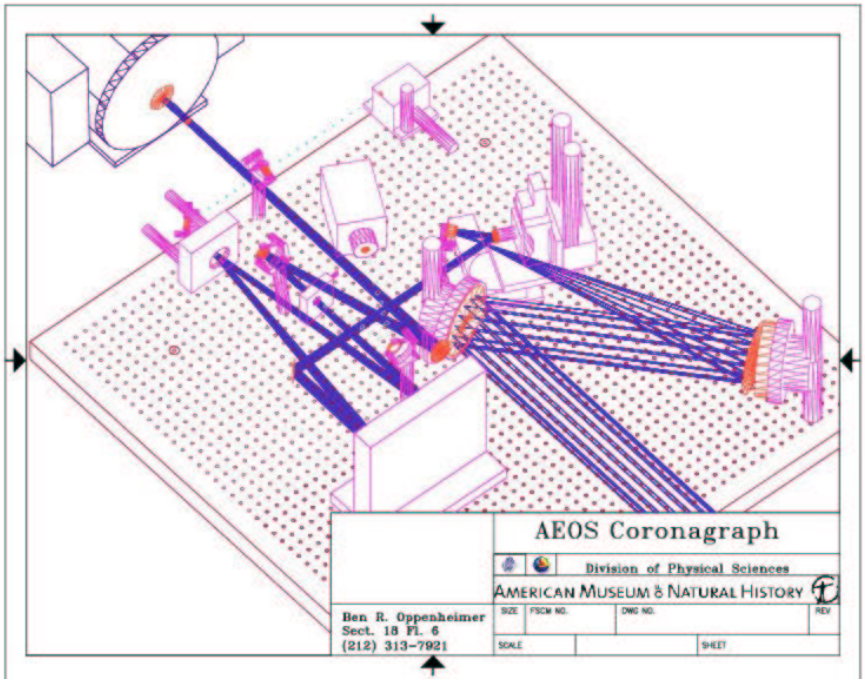

Fig. 4 Isometric projection of coronagraph optics train

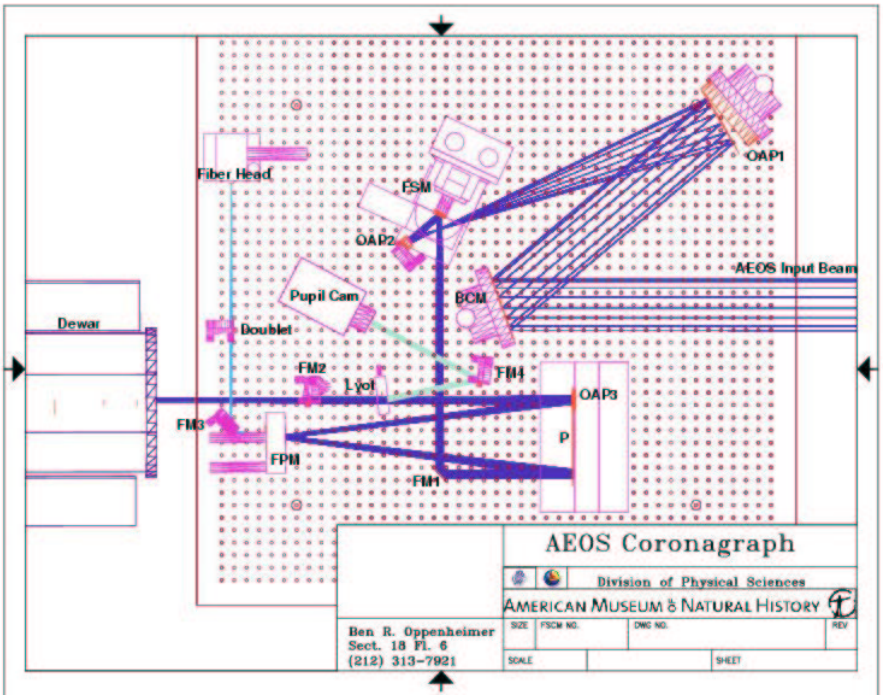

Fig. 5 Top-down view of optics design with components labeled

Fig. 4, an isometric projection of the optomechanical model of the instrument, is provided to make interpretation of Fig. 5 simpler. Fig. 5 shows the optical train from overhead with all of the optical elements labeled. An enclosure will be fitted around the entire breadboard to minimize air currents in the optical path. The design has the beam 6.25 inches above the breadboard surface or 8.45 inches above Room 6's optical bench surface. A 2.2 inch thick, 4 x 4 foot breadboard supports the entire instrument, except for the dewar. The table at AEOS is 12 x 4 feet. Its surface can be positioned at 37.75 to 38.5 inches above the room's floor, which places the beam at a height of between 8 and 8.75 inches above the table surface. The coronagraph requires the beam to be near the middle of this range. The optical bench will be floated during observations. The coronagraph optical train consists of the following pieces, all shown in Figure 5. Surface figures are quoted as peak-to-valley measurements at HeNe laser light.

BCM

The first optic (Beam Capture Flat or BCM) serves to capture the beam into the subsequently aligned path. BCM is at the reimaged telescope pupil. The optic is a 6 inch Zerodur λ/20 flat in a post-mounted kinematic mount. Placing BCM at the pupil plane is partly in anticipation of a possible upgrade of this instrument which would include a deformable mirror in the BCM location.

OAP1, OAP2 (Beam Compressor)

The beam is compressed by a factor of ten to a 10.48 mm diameter by two off-axis parabolae (OAP1 and OAP2). Beam compression is needed in order to permit the fast (2 kHz) tip/tilt system to be constructed at low cost. OAP1 is a 6 inch metal λ/20 optic with a 600 mm focal length, situated 200 mm off axis (giving an 18.42 degree angle to the beam). The center of the optic is 200 mm off-axis. OAP2 is a custom, 25.4 mm diamond-turned aluminum mirror with a gold over nickel coating. It has a 60 mm focal length and is 20 mm off-axis. This compensates the aberrations due to OAP1.

FSM

OAP2 reimages the pupil plane about 60 mm after reflection. The Fast Steering Mirror (FSM) is situated 2 cm further along the beam path. Ideally the tip/tilt correction should be done exactly in the pupil plane to prevent any motion of the pupil image itself. In this case though, let us examine the expected pupil image motion due to the movement of FSM. 0.1 arcsec of tip/tilt on the sky corresponds to 36.3 arcsec at the FSM (magnification is 363 from the primary to the FSM) or 175 μrad. If we allow a pupil misalignment of 0.1% of a 10 mm beam (10 μm), then 10 μm / 175 μrad gives 5.7 cm, which is the furthest the FSM can be situated from the pupil plane under this constraint. In truth, pupil misalignment up to a few percent of the beam diameter is permissible before substantial losses in dynamic range in the final image accrue [1]. Moving the FSM 2 cm past the pupil image results in substantial improvements in the clearance between FSM's mount and the beam, although it permits pupil motion of up to 0.03% of the beam diameter.

FSM is a 25.4 mm λ/20 Zerodur flat attached to a 25 mm aluminum flexure mount activated by a set of 4 PZT stacks. The mirror reflects the beam through a 50 degree angle (25 degree angle of incidence). The mount is attached to a spacing plate, which bolts into the faceplate of a goniometric cradle controlled with a stepper motor. This arrangement places the axis of rotation of the cradle at the center of the optic. The cradle is attached through a set of posts and thick plates to a rotation stage, also controlled with a stepper motor.

The PZT stacks can move the mirror ± 1 mrad (± 0.57 arcsec on the sky) at update rates over 2 kHz. The stacks, including the mount and a slightly larger mirror than the one we are using, have a resonant frequency of 2.4 kHz. Our electronics are capable of placing the star with an accuracy of 28 μas (0.12 nanorad) as measured on the sky (about 50 nanorad tilt error on the FSM). This substantially compensates the residual tilt error on the AEOS beam, currently measured at up to 200 milliarcsec.

The two other rotation stages are used for placing the star on the coronagraph's focal plane mask. These motors will be inactive when the tip/tilt loop is operating, although they could be used to offload the PZT stacks. The rotation stages have a precision of 3.6 arcsec or 17 μrad at the FSM optic. This translates to 10 mas on the sky. For reference, the focal plane masks are 275 to 500 mas in diameter (as projected on the sky).

Mounting the PZT stack on the heavy goniometric cradle and rotation stage ensures mechanical stability. The mount is over 10 times as massive as the active PZT stage.

FM1
Fold Mirror 1 (FM1) simply folds the beam. The current design has two fold mirrors in the science beam, necessary to keep the instrument within the spatial constraints of Room 6. FM1 is a 2 inch λ/20 Zerodur flat mounted in a post-raised gimbal mount.

P
The Parabola (P) on the lower right side of Figure 5 serves as the heart of a pseudo-Offner relay that reimages the star at the focal plane mask and the pupil at the Lyot stop. P is 8 inches in diameter (the beam incident on the mirror is contained within a 140 mm circle centered at P's center). P has a focal length of 600 mm. Surface accuracy for this optic is less stringent since the beam uses only a small region on opposite sides of the optical axis (λ/10). The 600 mm focal length provides an f/57.25 beam to the image mask.

FPM
The Focal Plane Mask (FPM, a. k. a. occulting mask) sits at the focus of P. The optical design provides perfect on-axis imaging at FPM, essentially required for an optimized, diffraction limited coronagraph. The focal plane mask is a diamond turned flat mirror 2 inches in diameter. A hole is drilled through the center of the optic and beveled on the back side. The hole, ranging from 275 to 500 μm in diameter, serves as the occulting mask. The starlight that passes through the hole is used to close the tip/tilt control loop. The f/57.25 beam results in a plate scale on the FPM of 993 μas / μm. This large f/# is necessary to avoid extremely expensive micromachining of these optics. Four FPMs will be made with holes to permit optimal occultation at all observing wavelengths.

The FPM is on a gimbal mount which is controlled with two DC servo motors. The servo motors can be used to precisely align the pupil with the Lyot stop. Furthermore, they can be operated to maintain pupil alignment whenever the telescope pupil is illuminated with a star. This is achieved with the pupil imaging camera (Pupil Cam) and a second control loop running along with the fast tip/tilt loop. Our science integrations will tend to be quite short (partly due to the lack of an image rotator and the alt/az design of AEOS). In light of this and the fact that beam wander in AEOS is relatively slow, pupil alignment can take place between exposures.

Lyot
The Lyot stop is exactly located at a plane conjugate to the telescope pupil. The pupil is reimaged without aberration here. The Lyot stop itself is a metal mirror, on the side facing P. The configuration shows it slightly tilted in the Figs. 4 and 5. This is a 6 degree angle meant to reflect the light of the star from the regions of the beam that are obscured by the Lyot stop into Pupil Cam, situated above the FPM in Fig. 5. The camera is focused on the Lyot stop and permits measurement of Lyot stop-to-telescope pupil alignment. The Lyot stop is also mounted on a rotation stage so that the spiders can be matched to the telescope spiders.

FM2
Gimbal mounted Fold Mirror (FM). 1 inch diameter λ/20 Zerodur, protected silver. This tilts the beam up away from the table and breadboard to feed the final focusing optic, OAP3.

OAP3
OAP3 is a diamond turned custom Off-Axis Parabola, 750 mm focal length, 2 inch diameter, gold over nickel coating, λ/20 surface, 270 mm off axis (measured to center of OAP3), mounted on a precision kinematic mount situated above the P mount.

This optic provides the final focus in front of the Dewar (the IR science camera). It is located one focal length away from the Lyot stop. The final beam entering the Dewar is F/71.34. This provides a plate scale of 14.73 mas/pixel at the detector. The current design also transmits a 49 mm diameter unvignetted FOV at the detector, while the actual detector spans 37 mm, providing a viewable field 30.178 arcsec on a side.

Tip/Tilt Optics (FM3, Doublet, Fiber head)
The tip/tilt optics provide a signal for the control of the tip/tilt loop, which should operate at an update frequency of 2 kHz. This necessitates an extremely fast detection method. Single photon counting modules (Avalanche PhotoDiodes) are presently the only suitable detectors. In our case, the limiting factor is the frame rate, not the number of photons available: Considering the throughput of the AEOS system in addition to the throughput to the

APDs, a sufficient number of photons can be detected in 0.5 ms from stars brighter than 4th magnitude in the 0.7 to 1 μm range (the range of sensitivity for the APDs) to provide a centroid with a precision of 57 μas. (The signal-to-noise requirement here is 800 for an image size of 45 mas, which is the diffraction limit at the signal wavelength.) For a 7th magnitude star, the centroiding error is approximately 400 μas. For the brightest stars, a neutral density filter may be required to prevent APD saturation.

Four APDs will serve as the tip/tilt detector, fed by a four-fiber bundle with a set of four lenslets on a single substrate positioned and aligned to the fiber heads. This "quad-cell" fiber pigtail will be placed inside a fiber head micropositioner actuated with two motors to provide x and y translation of the fiber head in the image plane. The image plane is formed with a doublet lens mounted behind the FPM (FM3 provides the needed clearance for the beam path). The motorized stage permits the system to track a star regardless of where the hole in FPM sits. The four fibers from the fiber pigtail are then connected directly into the APDs, which will be housed in the electronics rack enclosure.

The doublet forms an image of the FPM hole at the lenslet in front of the quadrant fiber head. The doublet has a 150 mm focal length, giving an Airy spot diameter of about 200 μm at the lenslet surface.

5. CURRENT PROJECT STATUS

The Kermit IR camera underwent first light observations using the engineering grade detector in April 2003. It functions well, with some minor issues that will be addressed before the first coronagraphic run later in 2003. In rather poor weather conditions (2" seeing in the optical), Kermit was able to make an image with a Strehl ratio of approximately 60% in the H band. This is particularly encouraging and seems to confirm the notion that a 90% Strehl will be achieved during median seeing conditions in the H-band [5].

The coronagraph is nearly complete and assembled in the astrophysics laboratory in New York. Custom optics and all off-the-shelf components are in hand. The alignment procedure is complete and software proceeds on schedule. We anticipate meeting the deadline to deliver the optics to Maui in late October or early November 2003.

6. REFERENCES

1. Sivaramakrishnan, A., Koresko, C. D., Makidon, R. B., Berkefeld, T., and Kuchner, M. J., Coronagraphy with High-Order Adaptive Optics, *Astrophysical Journal*, Vol. 552, 397-405, 2001.
2. Lyot, M. B., Study of the Solar Corona and Prominences without Eclipses, *Monthly Notices of the Royal Astronomical Society*, Vol. 99, 578-590, 1939.
3. Oppenheimer, B. R., Dekany, R. G., Hayward, T. L., Brandl, B., Troy, M., and Bloemhof, E. E., Companion Detection Limits with Adaptive Optics Coronagraphy, *Proceedings of SPIE*, Vol. 4007, 899-905, 2000.
4. Schroeder, D. J. et al, A Search for Faint Companions to Nearby Stars Using the Wide Field Planetary Camera 2, *Astronomical Journal*, Vol. 119, 906-922, 2000.
5. Perrin et al. this volume.